Energy-Storage-Based Intelligent Frequency Control of Microgrid With Stochastic Model Uncertainties

Chaoxu Mu, *Senior Member, IEEE*, Yong Zhang, Hongjie Jia, *Member, IEEE*, and Haibo He, *Fellow, IEEE*

***Abstract*—With the increasing proportion of renewable power generations, the frequency control of microgrid becomes more challenging due to stochastic power generations and dynamic uncertainties. The energy storage system (ESS) is usually used in microgrid since it can provide flexible options to store or release power energy. In this paper, an intelligent control strategy completely based on the adaptive dynamic programming (ADP) is developed for the frequency stability, which is designed to adjust the power outputs of micro-turbine and ESS when photovoltaic (PV) power generation is connected into the microgrid. Further, considering the changes of PV power and load demand in a day, the full utilization of PV power and the recycling of energy storage are realized through the proposed regulation strategy. Numerical simulation results validate the energy-storage-based intelligent frequency control strategy for the microgird with stochastic model uncertainties, and comparative studies based on PID, LQR and fuzzy logic control illustrate the superiority of the proposed control strategy.**

***Index Terms*—Frequency control, energy storage system (ESS), photovoltaic (PV) power, stochastic model uncertainties, adaptive dynamic programming (ADP), microgrid.**

I. Introduction

WITH the increasing of energy demand, the renewable energies have attracted wide attention, such as wind energy, water energy, solar energy, and so on. Among them, the photovoltaic (PV) power generation is a more common way to utilize the endless solar energy. However, it is unfortunate that the PV power is sensitive and even has large fluctuation in a cloudy day [1]–[3], which is hard to be predicted due to the difficulty of getting known when there are clouds above the PV arrays. Simultaneously, the power energy consumption is becoming more and more various. Thus, for a microgrid, when the renewable energy such as PV power generation is integrated, it is obvious that there are power mismatch and stochastic uncertainties. Meanwhile, during the transmission and measurement of mircogrid, the internal parameters such as the time constant of governor may randomly fluctuate within a small range of its nominal value [4], [5]. Therefore, these stochastic power mismatch and uncertainties are possible to cause the frequency instability, and bring unexpected trouble to the safe operation of microgrid [6]–[8].

The microgrid is actually complex with various power mismatch, which may lead to frequency fluctuation and bring negative impacts on the energy-using equipment. There are generally two approaches to deal with the problem. One is to decrease the power generation uncertainties. To a certain extent, more accurate scheduling plan can be achieved when the power generation prediction of renewable energy is reasonable, then the frequency fluctuation can be deduced by some power electronic techniques [8]–[12]. However, it requires the real-time prediction of power generation in frequency regulation, and is different from the prediction of entire power generation capacity. The accurate prediction of power generation is difficult due to the real-time varying factors of renewable energy power generation. For example, it is hard to predict when the clouds come above the PV arrays in a day-ahead dispatch. The other is to stabilize the frequency through control strategies. Many control methods have been applied for frequency regulation, such as proportion-integration-differentiation (PID) control [13], fuzzy logic control [14], [15], sliding mode control [16], [17], and so on.

Intelligent control has been developed for complex systems based on system data and learning-based methodologies. Adaptive dynamic programming (ADP) is an effective method with optimality by function approximation, especially for nonlinear systems and complex systems without system models. It can obtain the approximately optimal solution when facing the "curse of dimensionality" [18]–[20] by learning techniques, which is usually implemented by neural networks. Compared with PID, fuzzy logic control and so on, ADP is originated from dynamic programming, and has been widely investigated in many fields, such as the aspects of robotics, aircrafts, aerospace and navigation [21]–[23]. Furthermore, some improved ADP-based control strategies have been extended to cope with uncertain nonlinear systems [24]–[27]. Research results of ADP are relatively fruitful in power systems, which have been reported in many literatures [17], [28]–[31]. For example, an ADP-based control scheme was designed to assist the load frequency control of power system with sliding mode

Manuscript received August 13, 2018; revised November 16, 2018, March 4, 2019, June 3, 2019, and August 26, 2019; accepted September 7, 2019. Date of publication September 20, 2019; date of current version February 19, 2020. This work was supported in part by the National Natural Science Foundation of China under Grant 51625702 and Grant 61773284, and in part by the National Science Foundation under Grant ECCS 1917275. Paper no. TSG-01186-2018. *(Corresponding author: Haibo He.)*

C. Mu, Y. Zhang, and H. Jia are with the School of Electrical and Information Engineering, Tianjin University, Tianjin 300072, China (e-mail: cxmu@tju.edu.cn; zytju@foxmail.com; hjjia@tju.edu.cn).

H. He is with the Department of Electrical, Computer, and Biomedical Engineering, University of Rhode Island, Kingston, RI 02881 USA (e-mail: he@ele.uri.edu).

Color versions of one or more of the figures in this article are available online at http://ieeexplore.ieee.org.

Digital Object Identifier 10.1109/TSG.2019.2942770

control [17]. By using the adaptive critic design, a wide-area measurement based dynamic stochastic optimal power flow control algorithm was applied in a smart grid [28]. However, ADP is often designed as the supplementary control in the existing power system research, and it is rarely seen that the direct ADP control for power systems.

In power systems, the micro-turbine is considered as the controlled device to compensate the power mismatch and smooth frequency fluctuation. However, for microgrid with renewable energies, the micro-turbine should be assisted by some energy storage devices for more effective operations [32]. Due to the great performance of energy storage system (ESS), it has been widely used to improve the controllability of microgrid and provide flexible energy management solutions. In recent years, various energy storage systems have been investigated, such as battery energy storage station [33]–[35], flywheel storage system [36], and fuel cell/electrolyzer hybrid system [37], [38]. In the actual application of ESS, the state of charge (SOC) limits are important and considered as constraints [39]–[42].

It is inevitable that the power mismatch occurs between power generation and load demand. In this paper, both micro-turbine and ESS are used to restrain the frequency fluctuation in the design of intelligent frequency control, which provides the theoretical store for the application of future microgrid. Based on the large installed capacity of PV plants in a future microgrid, the efficient utilization of PV power is significantly concerned and an energy-storage-based scheduling strategy is proposed to absorb the superfluous PV power and compensate the insufficient power generation in the period of one day. This regulation strategy is investigated based on the day-ahead dispatch which does not need high accuracy compared with the intra-day dispatch. The main contributions of this paper are shown as follows. First, the microgrid with ESS is established by involving parameter uncertainties and generation rate constraint (GRC) of generator, stochastic PV power, SOC limits and power constraints of ESS. Second, an intelligent frequency control strategy is designed to adjust the power outputs of ESS and micro-turbine by using the robust ADP control, where the new cost function is defined with the bound of uncertainties. Third, the ESS is used to restrain the frequency fluctuation and dispatch the PV power to achieve full utilization. Through the rational design of two SOC limits, the recycling of ESS can be realized in the regulation strategy.

The rest of this paper is presented as follows. In Section II, the investigated microgrid is established. Section III designs the intelligent frequency control strategy based on ESS, which is implemented by neural networks. Simulation analysis is investigated to demonstrate the effectiveness of proposed control strategy through comparative studies in Section IV. Finally, some conclusions are summarized in Section V.

II. Benchmark Microgrid Description

A. ESS-Based Microgrid With Uncertainties

Considering the high permeability of PV power generation, the uncertainties need to be treated with caution. In this paper, the microgrid with PV power generation is investigated, which is composed of PV arrays, load demands, ESS and micro-turbine including governor. The detailed schematic diagram of microgrid is shown in Fig. 1. Similar to the description in [15] and [17], the transfer functions of equivalent micro-turbine, governor, ESS and power system are expressed as $G_t = 1/(T_t s+1), G_g = 1/((T_g+\sigma_g(t))s+1), G_e = 1/(T_e s+1), G_p = k_p/(T_p s+1)$, where T_g, T_t, T_e and T_p represent the time constants of governor, micro-turbine, ESS and system inertia, respectively. k_p is the gain coefficient of power system. It is noteworthy that the parameter of governor may change during the operation. Thus, the parameter uncertainty is reflected in the time constant T_g with $\sigma_g(t)$ in this paper.

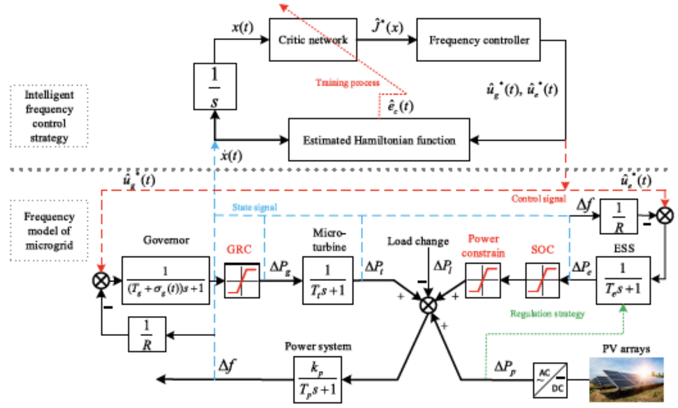

Fig. 1. Schematic diagram of benchmark microgrid with the intelligent frequency control strategy.

Define $x(t) = [\Delta f(t), \Delta P_t(t), \Delta P_g(t), \Delta P_e(t)]^T \in \mathbb{R}^m$ as the state vector of microgrid with the initial state $x(0)$, where $\Delta f(t)$ is the frequency deviation, $\Delta P_t(t)$ is the power output of micro-turbine, $\Delta P_g(t)$ is the governor position valve, and $\Delta P_e(t)$ is the power output of ESS. Then the frequency dynamics can be described by

$$\Delta\dot{f}(t) = \frac{k_p}{T_p}[\Delta P_t(t) + \Delta P_e(t) + \Delta P_p(t) - \Delta P_l(t)] - \frac{1}{T_p}\Delta f(t), \tag{1}$$

$$\Delta\dot{P}_t(t) = -\frac{1}{T_t}\Delta P_t(t) + \frac{1}{T_t}\Delta P_g(t), \tag{2}$$

$$\Delta\dot{P}_g(t) = -\frac{1}{RT_g}\Delta f(t) - \frac{1}{T_g}\Delta P_g(t) + \frac{1}{T_g}u_g(t) + \frac{\sigma_g(t)}{T_g\big(T_g+\sigma_g(t)\big)}\left[\frac{1}{R}\Delta f(t) + \Delta P_g(t) - u_g(t)\right], \tag{3}$$

$$\Delta\dot{P}_e(t) = -\frac{1}{RT_e}\Delta f(t) - \frac{1}{T_e}\Delta P_e(t) + \frac{1}{T_e}u_e(t), \tag{4}$$

where $\Delta P_l(t)$ and $\Delta P_p(t)$ represent the uncertainties resulted from load change and PV power generation, respectively. R is the speed regulation coefficient. Meanwhile, $u_g(t)$ and $u_e(t)$ are control signals of micro-turbine and ESS, respectively. To simplify the description, the parameter uncertain term in (3) is defined as $\lambda_g(t) = \sigma_g(t)/\big[T_g\big(T_g+\sigma_g(t)\big)\big]$.

Combined with the above formulas (1)–(4), the uncertainties in the microgrid are divided into parameter uncertainties related to $\lambda_g(t)$, power uncertainties related to $\Delta P_l(t)$ and

$\Delta P_p(t)$. From another perspective, these uncertainties can also be classified into matched and mismatched uncertainties, which are used in this paper with $\Lambda(t)$ for matched uncertainties and $\Pi(t)$ for mismatched uncertainties. Then, the frequency dynamics can be expressed in a compressed form as

$$\dot{x}(t) = Ax(t) + G(u(t) + \Lambda(t)) + \Pi(t) \tag{5}$$

with

$$A = \begin{bmatrix} -\frac{1}{T_p} & \frac{k_p}{T_p} & 0 & \frac{k_p}{T_p} \\ 0 & -\frac{1}{T_t} & \frac{1}{T_t} & 0 \\ -\frac{1}{RT_g} & 0 & -\frac{1}{T_g} & 0 \\ -\frac{1}{RT_e} & 0 & 0 & -\frac{1}{T_e} \end{bmatrix}, \quad G = \begin{bmatrix} 0 & 0 \\ 0 & 0 \\ \frac{1}{T_g} & 0 \\ 0 & \frac{1}{T_e} \end{bmatrix},$$

where A is the system matrix, G is the control matrix, and $u(t) = [u_g(t), u_e(t)]^T \in \mathbb{R}^n$ is the control input. Correspondingly, the matched and mismatched uncertainties are stated as

$$\Lambda(t) = \begin{bmatrix} -T_g\lambda_g(t)u_g(t) \\ 0 \end{bmatrix}, \Pi(t) = \begin{bmatrix} \frac{k_p}{T_p}(\Delta P_p(t) - \Delta P_l(t)) \\ 0 \\ \lambda_g(t)\left(\frac{1}{R}\Delta f + \Delta P_g(t)\right) \\ 0 \end{bmatrix}.$$

It should be noted that the nonlinear GRC is considered for the governor of micro-turbine referring to [7]. Meanwhile, the GRC is an important condition to constrain the rising and falling slew rate of position valve $\Delta P_g(t)$ of governor.

B. State of Charge Limit of ESS

In the ESS-based regulation strategy, the SOC limit of ESS is important when the energy storage equipment is connected to the power grid. The equipment loss or the SOC condition of ESS is often mentioned in some research works. Since the equipment loss is always related to the SOC condition of ESS, then in this paper, the SOC limit of ESS is considered in the process of optimization, as shown in Fig. 1.

The ESS in the microgrid takes actions in two scenes. One is to restrain the frequency fluctuation caused by parameter and power uncertainties. The other is to dispatch the PV power generation and fully utilize the solar energy. There are two defined SOC limits for ESS corresponding to different scenes.

We first define the SOC limit for restraining the frequency fluctuation. Let $Soc(t)$ be the state of charge and Soc^0 be the initial SOC of ESS. Then, we use $Ess1(t)$ to express the energy change at time t of the energy storage equipment. Therefore, the SOC limit is defined as follows:

$$Soc(t+1) = \begin{cases} Soc(t) - \int_0^t Ess1(\tau)d\tau, & Soc^m < Soc(t) < Soc^M, or \\ & Soc(t) = Soc^M \& Ess1(t) > 0, or \\ & Soc(t) = Soc^m \& Ess1(t) < 0, \\ Soc(t), & else, \end{cases} \tag{6}$$

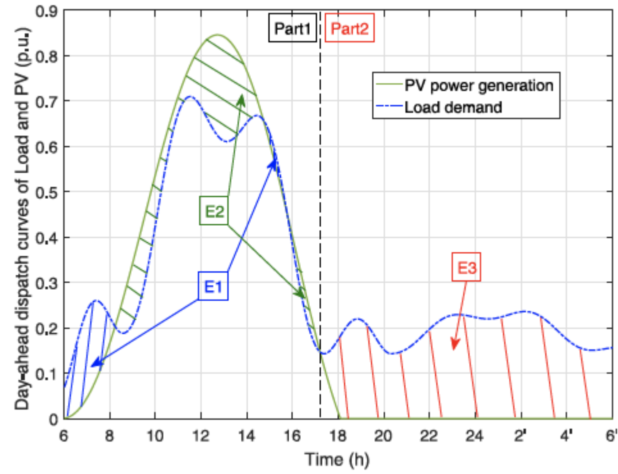

Fig. 2. Day-ahead dispatch curves of load demand and PV power.

$$Ess1(t) = \begin{cases} \Delta P_e^M/\beta, & \Delta P_e(t) > \Delta P_e^M, \\ \Delta P_e(t)/\beta, & 0 < \Delta P_e(t) \le \Delta P_e^M, \\ \beta\Delta P_e(t), & \Delta P_e^m \le \Delta P_e(t) \le 0, \\ \beta\Delta P_e^m, & \Delta P_e(t) < \Delta P_e^m, \end{cases} \tag{7}$$

where Soc^M and Soc^m are the upper and lower limits of SOC. Meanwhile, ΔP_e^M and ΔP_e^m are the upper and lower limits of ESS power constraints, respectively. β is the charging-discharging coefficient of ESS.

C. Sustainable Development and Recycling of ESS

In this subsection, the SOC limit is developed for dispatching the PV power and realizing the recycling of ESS. This SOC limit is defined based on the day-ahead dispatch curves of a commercial office building, as shown in Fig. 2.

In Fig. 2, 2′, 4′ and 6′ indicate the time of tomorrow. It can be observed that the whole process can be divided into two parts at a certain time instant. After that, the PV power is always lower than the load demand, marked as the red shadow area $E3$. Define the power deviation between load demand and the PV power as $Bias(t)$, which equals to the load demand minus the generated PV power. In Part 1, the blue shadow area $E1$ denotes the consumed ESS energy, and the green shadow area $E2$ illustrates the remaining PV energy stored into ESS. In Part 2, the stored energy by ESS is used to compensate the power consumption and the micro-turbine also generates the available power to supplement the remaining load demand. Let $Ess2(t)$ be the electric energy change of ESS in this scene. The SOC limit is defined as follows:

$$Soc(t+1) = \begin{cases} Soc(t) - \Phi(t)\int_0^t Ess2(\tau)d\tau, & Soc^m < Soc(t) < Soc^M, or \\ & Soc(t) = Soc^M \& Ess2(t) > 0, or \\ & Soc(t) = Soc^m \& Ess2(t) < 0, \\ Soc(t), & else, \end{cases} \tag{8}$$

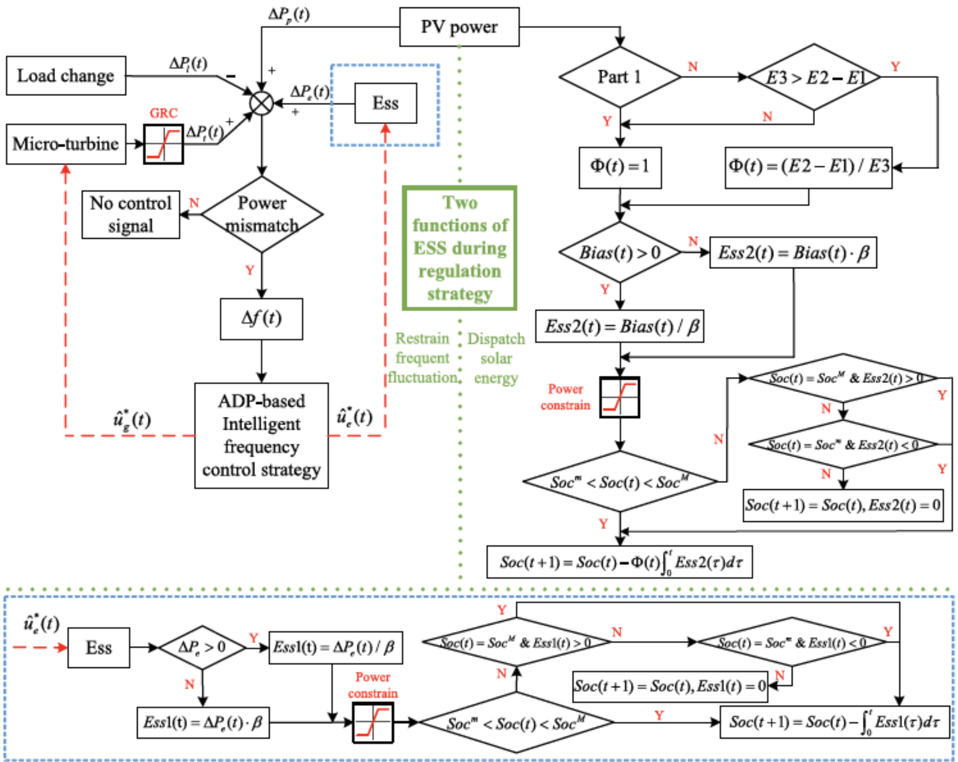

Fig. 3. Frequency regulation process under SOC limits.

where

$$Ess2(t) = \begin{cases} \Delta P_e^M/\beta, & Bias(t) > \Delta P_e^M, \\ Bias(t)/\beta, & 0 < Bias(t) \le \Delta P_e^M, \\ \beta Bias(t), & \Delta P_e^m \le Bias(t) \le 0, \\ \beta \Delta P_e^m, & Bias(t) < \Delta P_e^m, \end{cases} \tag{9}$$

$$\text{Part 1: } \Phi(t) = 1,$$

$$\text{Part 2: } \Phi(t) = \begin{cases} (E2 - E1)/E3, & E3 > (E2 - E1), \\ 1, & E3 \le (E2 - E1). \end{cases} \tag{10}$$

$\Phi(t)$ is designed as the regulating coefficient which is used to release the stored energy in the daytime. As shown in (10), we set $\Phi(t) = 1$ in Part 1 and dynamically adjust its value in Part 2. Under this definition of SOC limit, we can realize the dispatch of PV power and the recycling of ESS. It should be noticed that in (6) or (8), when we have $Soc(t+1) = Soc(t)$, the power output of ESS is set as $Ess1(t) = 0$ or $Ess2(t) = 0$.

During the frequency regulation, the uncertainties of governor parameter, load as well as PV power are considered, and the ESS is used to restrain uncertainties and fully utilize the PV power. The entire frequency regulation strategy is described in Fig. 3.

III. ADP-Based Intelligent Frequency Regulation

In this section, an intelligent frequency strategy is designed with the interior parameter uncertainties of governor and the external power uncertainties caused by load changes and stochastic PV power, which is regulated by the ADP method and implemented by neural networks.

As shown in Fig. 1, the intelligent frequency controller is designed to derive the effective control information from system data. The states of microgrid $\Delta f(t)$, $\Delta P_t(t)$, $\Delta P_g(t)$ and $\Delta P_e(t)$ are the inputs of frequency controller. Then, $\hat{u}_g^*(t)$ and $\hat{u}_e^*(t)$ are the approximately optimal control signals to be designed for adjusting the power outputs of micro-turbine and ESS. In the following, the design and implementation of intelligent control strategy will be presented.

A. ADP-Based Control Design

According to previous analysis, the frequency dynamics of studied benchmark microgrid is compressedly expressed by (5). Assume that the matched and mismatched terms are both upper bounded by $\|G\Lambda(t)\| \le \Gamma_\Lambda(t)$ and $\|\Pi(t)\| \le \Gamma_\Pi(t)$, respectively. For the frequency control, a state feedback control law $u(t)$ is designed to adjust the power outputs of micro-turbine and ESS, as shown in Fig. 1. The robust control for the uncertain frequency dynamic system (5) can be obtained by perusing the optimal control of its nominal system, which is formulated as

$$\dot{x}(t) = Ax(t) + Gu(t). \tag{11}$$

For the nominal system (11), we design the control law $u(t)$ by minimizing the cost function

$$J(x) = \int_t^\infty (U(x(\tau), u(\tau)) + \Theta(\tau))d(\tau), \tag{12}$$

where $U(x(t), u(t))$ is the utility function, chosen as $U(x(t), u(t)) = x^T(t)Qx(t) + u(t)^T Ru(t)$. Q and R are positive definite symmetric matrices with proper dimensions. $\Theta(t) \ge 0$ is the perturbed cost related to the uncertainties which is defined as

$$\Theta(t) = \theta_1^2\Gamma_\Lambda^2(t) + \theta_2^2\Gamma_\Pi^2(t) + \frac{\theta_1^2+\theta_2^2}{4\theta_1^2\theta_2^2}\|\nabla J(x)\|^2, \tag{13}$$

with $\nabla J(x) = \partial J(x)/\partial x$. θ_1 and θ_2 are the given constants corresponding to matched and unmatched uncertainties, respectively. The optimal cost function is defined as

$$J^*(x) = \min_{u\in\Omega_c}\int_t^\infty (U(x(\tau), u(\tau)) + \Theta(\tau))d\tau. \tag{14}$$

Based on the Bellman optimality principle, the Hamiltonian function can be obtained as

$$\begin{aligned}&H(x(t), u(t), \nabla J(x))\\ &\quad= (\nabla J(x))^T\dot{x}(t) + U(x(t), u(t)) + \Theta(t),\end{aligned} \tag{15}$$

and the optimal control law $u^*(t)$ satisfies the Hamilton-Jacobi-Bellman (HJB) equation

$$0 = \min_{u\in\Omega_c} H\big(x(t), u(t), \nabla J^*(x)\big), \tag{16}$$

where Ω_c is an admissible control set. Thus, the optimal frequency control law for system (11), i.e., the available robust control law for regulating frequency of uncertain benchmark system (5), can be derived as

$$u^*(t) = -\frac{1}{2}R^{-1}G^T\nabla J^*(x). \tag{17}$$

Bring the optimal control law (17) into (16), then the HJB equation is further transformed into the following form

$$\begin{aligned}0 &= (\nabla J(x))^T\dot{x}(t) + U(x(\tau), u(\tau)) + \Theta(t)\\ &= (\nabla J(x))^T Ax(t) - \frac{1}{4}(\nabla J(x))^T GR^{-1}G^T\nabla J(x)\\ &\quad + x(t)^T Qx(t) + \Theta(t),\end{aligned} \tag{18}$$

where the optimal HJB equation conforms to $0 = H(x(t), u^*(t), \nabla J^*(x))$ with the optimal frequency control law $u^*(t)$. Note that the optimal control $u^*(t)$ of nominal system (11) can achieve the effective robust control for uncertain benchmark system (5), which results from the new-defined cost function (12) including the perturbed cost and more explanation can refer to [43].

B. Iteration Algorithm for Approximating Optimal Control

Generally speaking, (18) is almost impossible to be directly solved due to partial differential terms. Hence, the iteration algorithm is applied to get the approximate solution of $u^*(t)$ and the optimal cost function $J^*(x)$ in (14). The algorithm flow of approximating the optimal solution is shown as follows.

Based on this iteration procedure, the iteration control law $u^{(i+1)}(t)$ would approximately converge to the optimal control law $u^*(t)$, and the iteration cost function $J^{(i+1)}(x)$ also converges to the optimal value $J^*(x)$ as the iteration index i goes to large enough [18]. In the following, based on the function approximation technique, the iteration algorithm is implemented by neural networks.

Algorithm 1 Solving the Approximate Optimal Control of Nominal System

a **Initialization:** Set the iteration index $i = 0$ and let $J^{(i)}(x) = 0$. Define a sufficiently small positive number ϱ as the prerequisite to stop the algorithm. Start the iteration from an initial admissible control law $u^{(0)}(t)$.

b **Iterative process:** Substitute the initial value $u^{(0)}(t)$ into (19) with $J^{(0)}(x) = 0$ in the first iteration. Then, $J^{(i+1)}(x)$ can be solved by

$$\begin{aligned}0 =&(\nabla J^{(i+1)}(x))^T\big(Ax(t) + Gu^{(i)}(t)\big)\\ &+ U(x(t), u^{(i)}(t)) + \Theta(t).\end{aligned} \tag{19}$$

c **Update control law:** Update the control law $u^{(i+1)}(t)$ based on the following formula

$$u^{(i+1)}(t) = -\frac{1}{2}R^{-1}G^T\nabla J^{(i+1)}(x). \tag{20}$$

d **Stopping Criterion:** If $\|J^{(i+1)}(x) - J^{(i)}(x)\| < \varrho$ is satisfied, stop the iteration and let $u^{(i+1)}(t)$ be the approximately optimal control law. Else, set $i = i + 1$ and return step b to the next iteration.

C. Neural Network Implementation of Intelligent Frequency Control

For realizing the iteration algorithm in Section III-B, single-hinder-layer neural networks are applied for approximating the control law and the cost function. Therefore, the optimal cost function in (14) is restructured with an ideal weight w_c as

$$J^*(x) = w_c^T\psi(x) + \nu_c(x), \tag{21}$$

where $w_c \in \mathbb{R}^j$ and j is the neuron number in the hidden layer, $x(t)$ is used as the neural network input, and $J^*(x)$ is the output. $\psi(x)$ is the activation function and $\nu_c(x)$ is the reconstruction error of neural network. For the cost function (21), we can obtain the partial derivative of $J^*(x)$ along $x(t)$, which is expressed as

$$\nabla J^*(x) = \nabla\psi^T(x)w_c + \nabla\nu_c(x), \tag{22}$$

with $\nabla\psi(x) = \partial\psi(x)/\partial x$ and $\nabla\nu_c(x) = \partial\nu_c(x)/\partial x$. Then, substitute (22) into (15) to get the Hamiltonian function

$$\begin{aligned}&H\big(x(t), u^*(t), w_c\big)\\ &= \big(\nabla\psi^T(x)w_c + \nabla\nu_c(x)\big)^T\dot{x} + U(x(t), u(t)) + \Theta(t)\\ &= \big(\nabla\psi^T(x)w_c + \nabla\nu_c(x)\big)^T\dot{x} + U(x(t), u(t)) + \theta_1^2\Gamma_\Lambda^2(t)\\ &\quad + \theta_2^2\Gamma_\Pi^2(t) + \frac{\theta_1^2+\theta_2^2}{4\theta_1^2\theta_2^2}\|\nabla\psi^T(x)w_c + \nabla\nu_c(x)\|^2,\end{aligned} \tag{23}$$

where $\nabla\nu_c^T(x)\dot{x}$ is the residual error which can be omitted in the Hamiltonian function when the weight training process is sufficiently enough.

In fact, the ideal weight w_c is unknown in the neural network approximation, thus an estimated weight $\hat{w}_c(t)$ is applied, and the approximate optimal cost function $\hat{J}^*(x)$ can be obtained as

$$\hat{J}^*(x) = \hat{w}_c^T(t)\psi(x). \tag{24}$$

Similarly, according to (22), $\nabla J^*(x)$ can also be approximated as

$$\nabla\hat{J}^*(x) = \nabla\psi^T(x)\hat{w}_c(t). \tag{25}$$

Therefore, by substituting (24) into (15), the estimated Hamiltonian function can be obtained as

$$\begin{aligned} &H\big(x(t), u^*(t), \hat{w}_c(t)\big) \\ &= \big(\nabla\psi^T(x)\hat{w}_c(t)\big)^T\dot{x} + U\big(x(t), u^*(t)\big) + \theta_1^2\Gamma_\Lambda^2(t) \\ &\quad + \theta_2^2\Gamma_\Pi^2(t) + \frac{\theta_1^2+\theta_2^2}{4\theta_1^2\theta_2^2}\|\nabla\psi^T(x)\hat{w}_c(t)\|^2 \\ &= \hat{e}_c(t). \end{aligned} \tag{26}$$

Based on (17) and (25), the approximately optimal frequency controller for system (11) can be obtained by using neural network approximation

$$\hat{u}^*(t) = -\frac{1}{2}R^{-1}G^T\nabla\psi^T(x)\hat{w}_c(t). \tag{27}$$

Take the estimated Hamiltonian function $H(x(t), u^*(t), \hat{w}_c(t))$ as the critic network error $\hat{e}_c(t)$, and define $E_c(t)$ with $\hat{e}_c(t)$ for regulating the critic network weight, which is

$$E_c(t) = \frac{1}{2}\hat{e}_c^T(t)\hat{e}_c(t). \tag{28}$$

By minimizing (28), the weight updating law can be designed as

$$\begin{aligned} \dot{\hat{w}}_c(t) &= -\gamma_c\frac{\partial E_c(t)}{\partial\hat{w}_c(t)} + \gamma_a\nabla\psi(x)GR^{-1}G^T\nabla J_s(x) \\ &= -\gamma_c\hat{e}_c(t)\nabla\psi(x)Ax(t) + \gamma_a\nabla\psi(x)GR^{-1}G^T\nabla J_s(x) \\ &\quad - \gamma_c\hat{e}_c(t)\frac{\theta_1^2+\theta_2^2}{2\theta_1^2\theta_2^2}\nabla\psi(x)\nabla\psi^T(x)\hat{w}_c(t) \\ &\quad + \frac{1}{2}\gamma_c\hat{e}_c(t)\nabla\psi(x)GR^{-1}G^T\nabla\psi^T(x)\hat{w}_c(t), \end{aligned} \tag{29}$$

where $\gamma_c > 0$ is the primary learning rate of critic network and $\gamma_a > 0$ is the auxiliary learning rate. $J_s(x) = 0.5x^T(t)x(t)$ is selected based on Lyapunov theorem.

Therefore, the estimated weight of critic network can be obtained by using the weight updating law (29). It means that (27) can provide the robust frequency control law for benchmark system (5) which has been implemented and the frequency can be stabilized under the stochastic uncertainties of parameters, power generations and loads.

Remark 1: Some learning-based adaptive control has been investigated in previous works, i.e., [17], [44], [45]. In [17] and [44], together with the SMC and PID controller, the ADP method was designed as the supplementary controller to give the auxiliary control signal for load frequency control of power system. In [45], based on the Hammerstein network identification of hybrid energy storage, a PID-type neural network controller was designed to adjust the frequency fluctuation and the tie-line power. Compared with these previous adaptive control scheme, the adaptive frequency control in this paper is directly obtained from the ADP method, but not the supplementary control. Moreover, by considering the renewable PV power, the energy-storage-based regulation strategy can reduce the waste of solar energy and achieve the sustainable utilization of ESS. These is also the obvious difference between this paper and previous works.

Remark 2: The two main work of this paper is regard to the day-ahead operation scheduling and the inter-day frequency control. The day-ahead operation curves of load demand and PV power are shown in Fig. 2. ESS is designed to store the remaining PV power during the day, thereby reducing the waste of PV power, and compensating load demand at the low stage of PV power. By using the regulation strategy of this paper, the SOC can meet the set value and realize the recycling of ESS. The real-time frequency regulation under various uncertainties are shown in Figs. 6–8, where the proposed ADP-based intelligent control strategy is used to adjust the power output of micro-turbine and ESS and restrain the frequency fluctuation.

TABLE I
PARAMETERS IN THE MICROGRID SYSTEM

Parameters	T_g	T_t	T_e	T_p	k_p	R
Values	0.3	0.3	0.5	10	1	0.08

TABLE II
CONSTRAINT CONDITIONS

Name	Variables	Values
Initial SOC	Soc^0	0.5
Upper limit of SOC	Soc^M	0.9
Lower limit of SOC	Soc^m	0.15
Charging-discharging coefficient	β	0.9
Upper limit power constraint of ESS	ΔP_e^M	0.15
Lower limit power constraint of ESS	ΔP_e^m	-0.15

IV. Simulation and Analysis

Based on the given day-ahead dispatch curves of commercial office building in Fig. 2, simulation is executed on the benchmark microgrid to restrain the frequency stability under stochastic model uncertainties and realize energy scheduling and sustainable utilization. For the micro-turbine, the nonlinear GRC condition of governor is considered with rising/falling slew rates [7], [46], [47], and it is specified as 10% per minute. Meanwhile, the power constraints of ESS are also considered during frequency regulation [40]. The parameters of microgrid are shown in Table I. The commercial office building has the rated capacity of 225 kW and the PV rated capacity is 250 kW. The parameters of SOC limits and the power constraints of ESS are shown in Table II.

In the intelligent frequency control strategy, the used parameters are as follows, $Q = 2.5I_{4\times4}$, $R = 8.5I_{2\times2}$, $\theta_1 = 0.5$, $\theta_2 = 0.5$, $\gamma_c = 1.0$, and $\gamma_a = 0.1$, where I is the identity matrix. Based on system data, the weights of critic network can be obtained after training, which is shown in Fig. 4. These weights converge to $\hat{w}_c = [0.0387, -0.0352, 0.0285, 0.0732, 0.1300, -0.2455, -0.4023, 0.3213, 0.3968, 0.4944]^T$ and they are applied to get the frequency controller according to (27). During the training, with randomly persistent disturbance excitation, the frequency deviation $\Delta f(t)$, the micro-turbine power output $\Delta P_t(t)$, the governor position valve $\Delta P_g(t)$, and the ESS power output $\Delta P_e(t)$ finally converge to zero, as shown in Fig. 5.

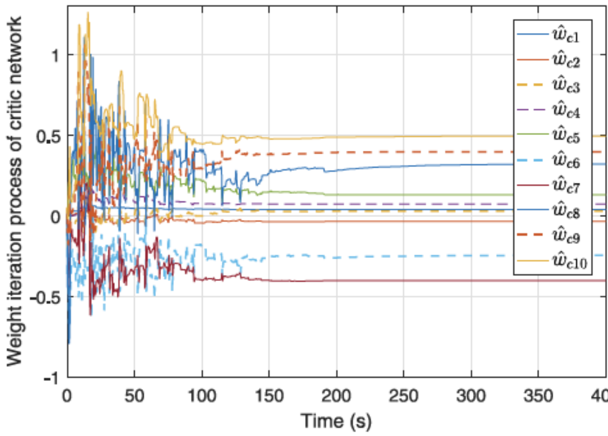

Fig. 4. Weight convergence in the training process.

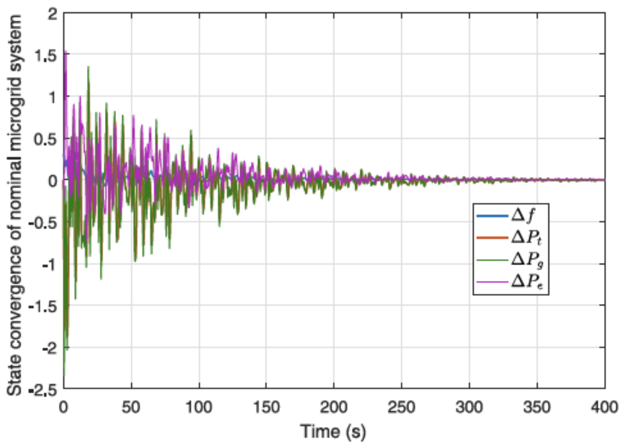

Fig. 5. State convergence of nominal microgrid system with persistent excitation condition.

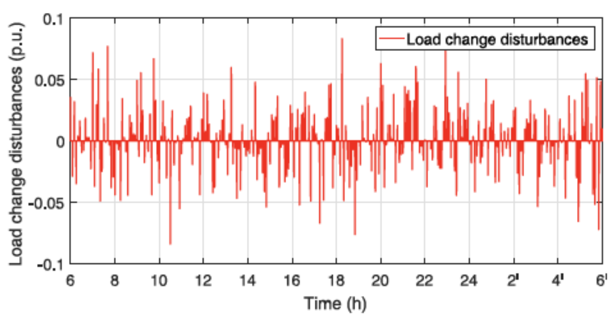

Fig. 6. Load change disturbances.

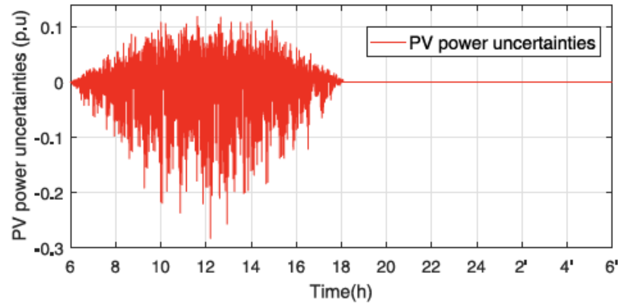

Fig. 7. PV power uncertainties.

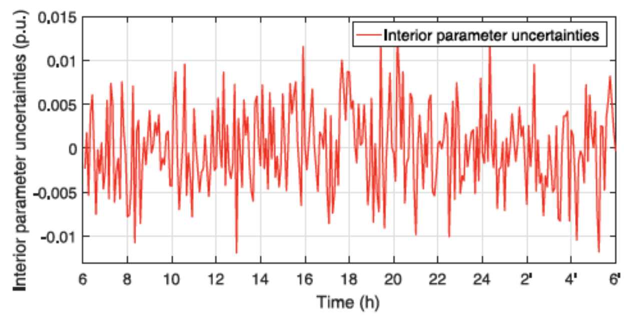

Fig. 8. Parameter uncertainties of the governor.

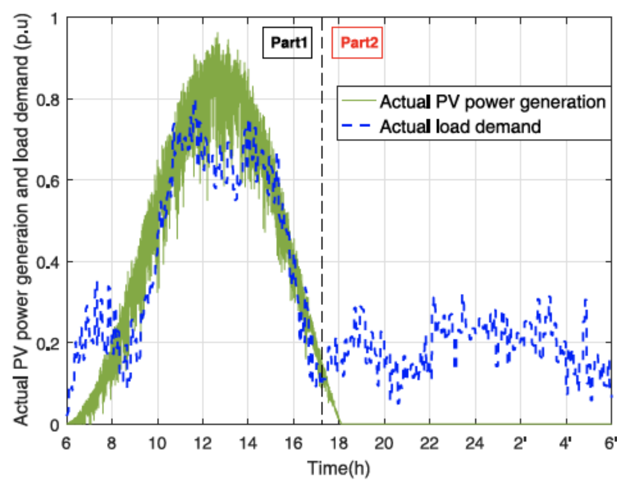

Fig. 9. Actual PV power generation and load demand in a day.

A. Under PV Power Uncertainties and Load Changes

Consider that the PV power is connected to the microgrid. The actual load demand and PV power are always different from the scheduled power in the day-ahead dispatch. The load change disturbances are shown in Fig. 6, and the PV power uncertainties affected by environmental conditions are reflected in Fig. 7. Two main influence factors of PV power, irradiance and temperature, are considered here. As the clouds are time varying for PV arrays, the PV power is hard to predicted when there are cloudy above the PV arrays. Therefore, in the day-ahead dispatch, the PV power is predicted without considering the clouds or the cloudy weather. When the clouds come above the PV arrays, it reduces the irradiance and thus is dealt as the negative PV power uncertainties. The temperature change maybe cause positive or negative uncertainties. The irradiance is a more important factor than the temperature for PV power generation [48]–[51], therefore there are much more negative uncertainties than positive uncertainties. The parameter uncertainties of governor are considered as shown in Fig. 8. Then, the actual PV power generation and load demand in a day are shown in Fig. 9.

Under the stochastic model uncertainties shown in Figs. 6–9, the designed intelligent frequency controller is applied to keep the frequency stability of microgrid. For better showing the control performance, fuzzy logic control, linear quadratic regulator (LQR) and PID control are used as the

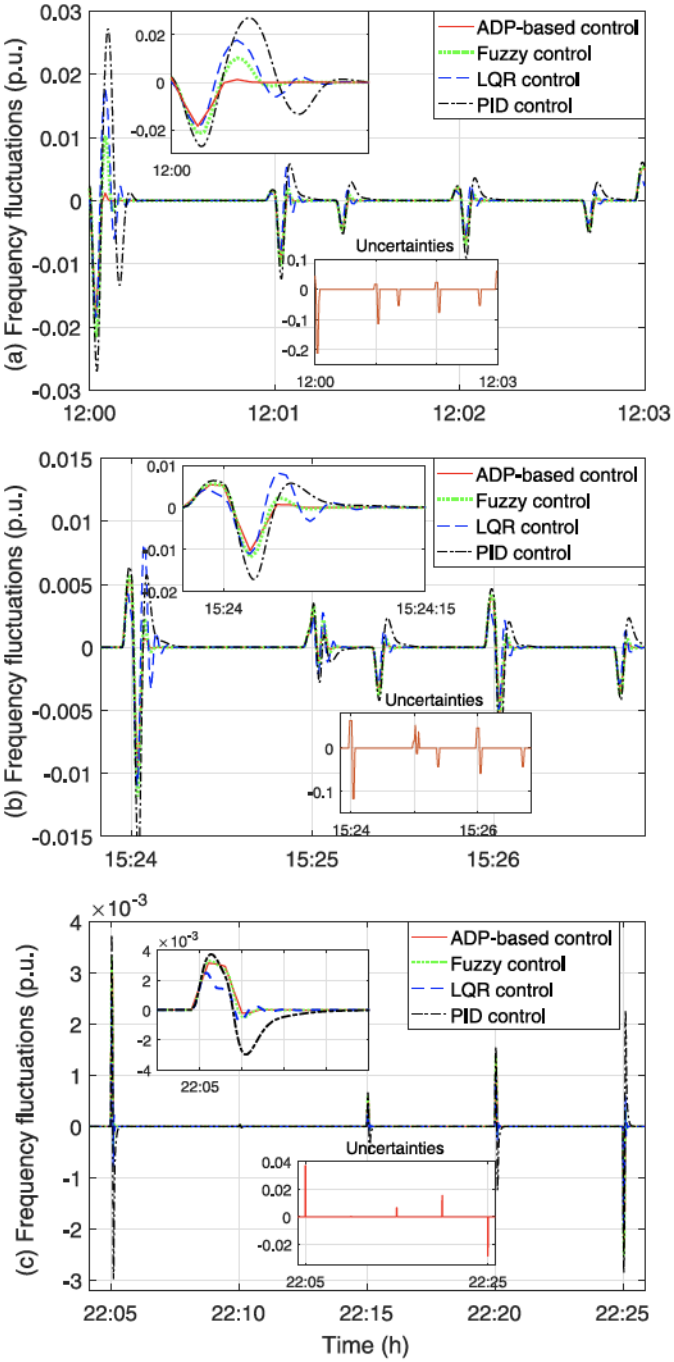

Fig. 10. Frequency regulation performance under stochastic model uncertainties.

comparative methods. The fuzzy rules used in this paper can be found in reference [52], where the scaling factors are designed as $K_e = 10$, $K_{ec} = 1$ and $K_u = 0.1$ with one input and two outputs. The parameters of PID controllers are shown in Table III. The LQR controller is designed as $u(t) = -kx(t)$, where the quadratic cost is consistent with (12), and the related matrices are given the same values. Then, the gain matrix k can be solved as

$$k = \begin{bmatrix} -0.8360 & 0.0754 & 0.2020 & 0.0102 \\ 0.5789 & 0.0267 & 0.0061 & 0.1627 \end{bmatrix}$$

TABLE III
PARAMETERS OF PID CONTROLLERS

Control signals	P	I	D
u_t	3.5	-1.2	0.1
u_e	3.1	-1.2	0.09

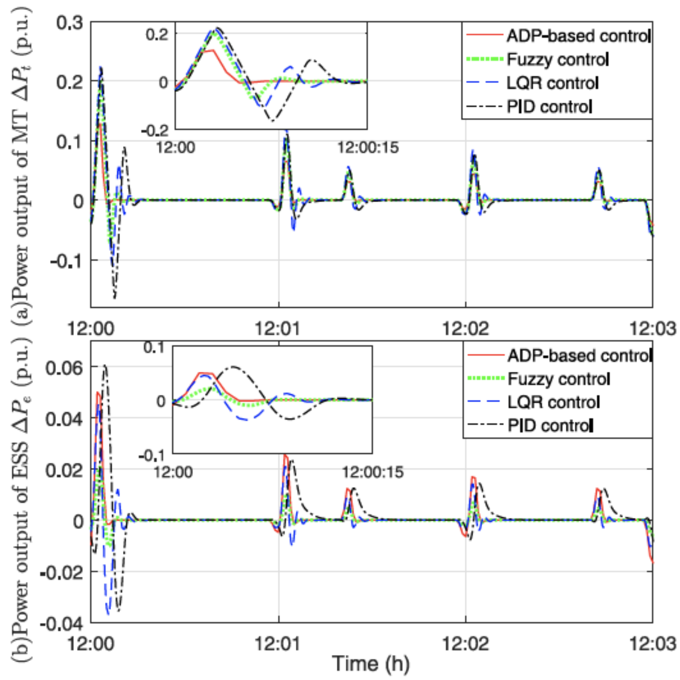

Fig. 11. Power outputs of micro-turbine and ESS under stochastic model uncertainties.

In Fig. 10, the frequency regulation in a day is shown to demonstrate the superiority of intelligent frequency control strategy. It can be seen that the ADP-based intelligent control method can better restrain the frequency deviations with fewer oscillations, compared with fuzzy control and PID control. The frequency deviations are also faster to be stabilized to zero with this intelligent control strategy. The control performance of LQR is similar with the ADP-based intelligent control when the frequency deviations are small since it is a linear optimal control method. However, in the case of large deviations, its performance becomes weaker than the ADP-based control, which is more obvious shown in Section IV-B. Meanwhile, we provide the power outputs of micro-turbine and ESS from 12:00 to 12:03 in Fig. 11 corresponding to Fig. 10(a), which are the control actions under ADP-based control, fuzzy control, LQR and PID control. It shows the required power outputs for micro-turbine and ESS in the frequency regulation to realize the control performance in Fig. 10(a). We take Fig. 10(a) as an example here and provide its analysis, which is similar to Figs. 10(b) and 10(c).

The ESS plays two roles in the regulation strategy: maintaining the frequency stability and dispatching the PV power. The ESS is applied during the whole frequency regulation process. The ESS dispatches the PV power to achieve its full utilization, as shown in Fig. 12, where the stored energy in Part 1 is consumed in Part 2. Thus, we can achieve the recycling and sustainable utilization of ESS where the final

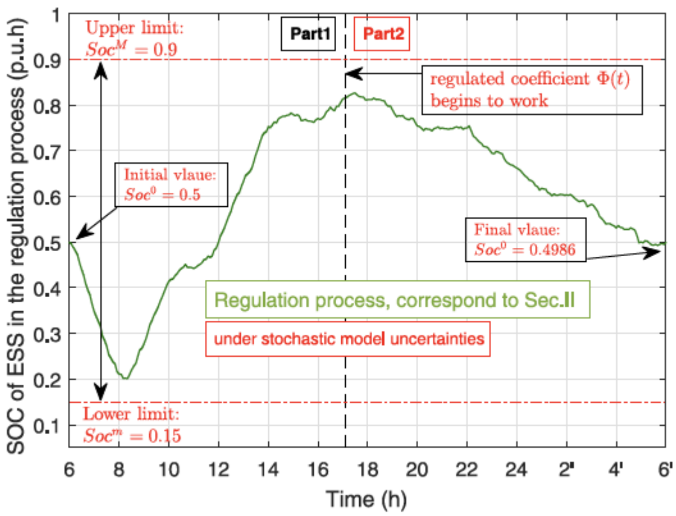

Fig. 12. SOC changes of ESS in a day.

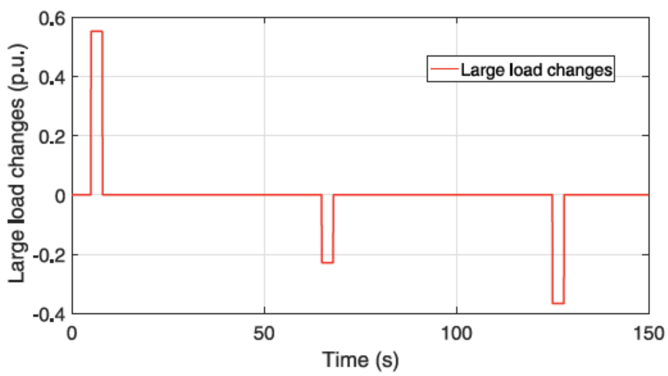

Fig. 13. Abnormal operation of large load changes.

value of SOC is basically equal to the initial value. The peak value of SOC reaches 0.82 $p.u.h$, thus the rated capacity of ESS is $0.82/0.9 * 250 \approx 228$ kWh. Considering the certain redundancy, the rated capacity of ESS can be selected as 235 kWh.

B. Under Large Load Changes

The normal operation of microgrid under PV power uncertainties and load changes has been investigated in Section IV-A. However, there may be sudden load fluctuations, such as the line faults and large load incorporation. As shown in Fig. 13, we investigated the large load changes, even more than 0.55 p.u. Then, from Fig. 14, it is obvious that the ADP intelligent control scheme performs better than fuzzy control, LQR control and PID control for dealing with large load changes.

In this sudden scenario, it can be seen in Fig. 14 that the PID control has poor performance for such large disturbances. Fuzzy control can work, but its performance becomes worse due to the fixed design of fuzzy rules. Since LQR control is a linear optimal control method designed for linear systems, the emergence of stochastic model uncertainties may lead to bad presentation in both robustness and convergence speed compared with the ADP-based control strategy. Large power changes may lead to frequency fluctuation and cause security

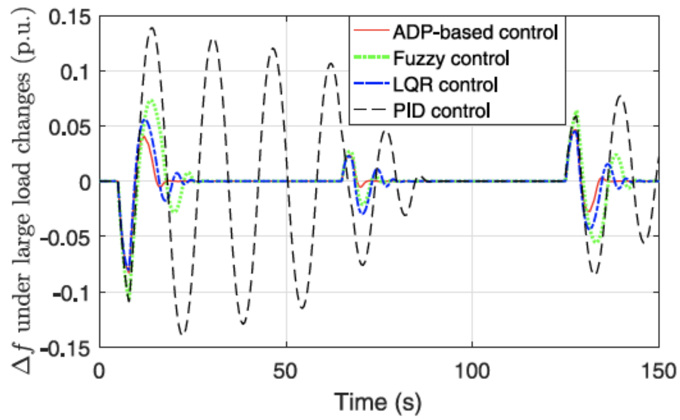

Fig. 14. Frequency regulation performance under large load changes.

risks. Therefore, the adaptability and robustness of controller is important for the microgrid system. The ADP-based intelligent control can be well adaptive when the microgrid is facing with various disturbances.

V. Conclusion

In this paper, we investigate the frequency control of microgrid with parameter, PV power and load uncertainties. An ADP-based intelligent control strategy is designed to adjust the power outputs of micro-turbine and ESS to restrain the frequency fluctuation. Further, the energy-storage-based regulation strategy is proposed to deal with the frequency control problem and dispatch the PV power to realize the recycling of ESS. In the regulation process, we can conclude that the proposed intelligent frequency control strategy can better adjust the frequency fluctuation compared with fuzzy control, LQR control and PID control. At the same time, the SOC of ESS can reach the desired state. This also reflects the rationality of regulation strategy. In the future, the topological network of microgrid can be considered, and more application scenarios can be introduced to extend this work.

References

[1] N. Kakimoto, S. Takayama, H. Satoh, and K. Nakamura, "Power modulation of photovoltaic generator for frequency control of power system," *IEEE Trans. Energy Convers.*, vol. 24, no. 4, pp. 943–949, Dec. 2009.

[2] N. Liu, M. Cheng, X. Yu, J. Zhong, and J. Lei, "Energy-sharing provider for PV prosumer clusters: A hybrid approach using stochastic programming and Stackelberg game," *IEEE Trans. Ind. Electron.*, vol. 65, no. 8, pp. 6740–6750, Aug. 2018. doi: 10.1109/TIE.2018.2793181.

[3] H. Jia *et al.*, "Coordinated control for EV aggregators and power plants in frequency regulation considering time-varying delays," *Appl. Energy*, vol. 210, pp. 1363–1376, Jan. 2018.

[4] H. J. Lee, J. B. Park, and Y. H. Joo, "Robust load-frequency control for uncertain nonlinear power systems: A fuzzy logic approach," *Inf. Sci.*, vol. 176, no. 23, pp. 3520–3537, 2006.

[5] R. K. Sahu, S. Panda, and U. K. Rout, "DE optimized parallel 2-DOF PID controller for load frequency control of power system with governor dead-band nonlinearity," *Int. J. Elect. Power Energy Syst.*, vol. 49, pp. 19–33, Jul. 2013.

[6] H. Asano, K. Yajima, and Y. Kaya, "Influence of photovoltaic power generation on required capacity for load frequency control," *IEEE Trans. Energy Convers.*, vol. 11, no. 1, pp. 188–193, Mar. 1996.

[7] G.-Q. Zeng, X.-Q. Xie, and M.-R. Chen, "An adaptive model predictive load frequency control method for multi-area interconnected power systems with photovoltaic generations," *Energies*, vol. 10, no. 11, p. 1840, 2017.

[8] R. Kadri, J.-P. Gaubert, and G. Champenois, "An improved maximum power point tracking for photovoltaic grid-connected inverter based on voltage-oriented control," *IEEE Trans. Ind. Electron.*, vol. 58, no. 1, pp. 66–75, Jan. 2011.

[9] K. Kobayashi, I. Takano, and Y. Sawada, "A study of a two stage maximum power point tracking control of a photovoltaic system under partially shaded insolation conditions," *Solar Energy Mater. Solar Cells*, vol. 90, nos. 18–19, pp. 2975–2988, 2006.

[10] T. Esram and P. L. Chapman, "Comparison of photovoltaic array maximum power point tracking techniques," *IEEE Trans. Energy Convers.*, vol. 22, no. 2, pp. 439–449, Jun. 2007.

[11] A. I. Dounis, P. Kofinas, C. Alafodimos, and D. Tseles, "Adaptive fuzzy gain scheduling PID controller for maximum power point tracking of photovoltaic system," *Renew. Energy*, vol. 60, pp. 202–214, Dec. 2013.

[12] W. Xu, C. Mu, and J. Jin, "Novel linear iteration maximum power point tracking algorithm for photovoltaic power generation," *IEEE Trans. Appl. Supercond.*, vol. 24, no. 5, pp. 1–6, Oct. 2014.

[13] S. Sukumar, M. Marsadek, A. Ramasamy, H. Mokhlis, and S. Mekhilef, "A fuzzy-based PI controller for power management of a grid-connected PV-SOFC hybrid system," *Energies*, vol. 10, no. 11, p. 1720, 2017.

[14] M. Veerachary, T. Senjyu, and K. Uezato, "Neural-network-based maximum-power-point tracking of coupled-inductor interleaved-boost-converter-supplied PV system using fuzzy controller," *IEEE Trans. Ind. Electron.*, vol. 50, no. 4, pp. 749–758, Aug. 2003.

[15] M. Datta, T. Senjyu, A. Yona, T. Funabashi, and C.-H. Kim, "A frequency-control approach by photovoltaic generator in a PV-diesel hybrid power system," *IEEE Trans. Energy Convers.*, vol. 26, no. 2, pp. 559–571, Jun. 2011.

[16] M. Klimontowicz, A. Al-Hinai, and J. C.-H. Peng, "Optimal LFC SMC for three–area power system with high penetration of PV," *J. Elect. Syst.*, vol. 12, no. 1, pp. 68–84, 2016.

[17] C. Mu, Y. Tang, and H. He, "Improved sliding mode design for load frequency control of power system integrated an adaptive learning strategy," *IEEE Trans. Ind. Electron.*, vol. 64, no. 8, pp. 6742–6751, Aug. 2017.

[18] P. J. Werbos, "Approximate dynamic programming for real-time control and neural modeling," in *Handbook of Intelligent Control: Neural, Fuzzy, and Adaptive Approaches*. New York, NY, USA: Van Nostrand Reinhold, 1992.

[19] F. L. Lewis and D. Liu, *Reinforcement Learning and Approximate Dynamic Programming for Feedback Control*. Hoboken, NJ, USA: Wiley, 2013.

[20] H. He, Z. Ni, and J. Fu, "A three-network architecture for on-line learning and optimization based on adaptive dynamic programming," *Neurocomputing*, vol. 78, no. 1, pp. 3–13, 2012.

[21] W. He, Y. Dong, and C. Sun, "Adaptive neural impedance control of a robotic manipulator with input saturation," *IEEE Trans. Syst., Man, Cybern., Syst.*, vol. 46, no. 3, pp. 334–344, Mar. 2016.

[22] Z. Ni, H. He, J. Wen, and X. Xu, "Goal representation heuristic dynamic programming on maze navigation," *IEEE Trans. Neural Netw. Learn. Syst.*, vol. 24, no. 12, pp. 2038–2050, Dec. 2013.

[23] C. Mu, Z. Ni, C. Sun, and H. He, "Air-breathing hypersonic vehicle tracking control based on adaptive dynamic programming," *IEEE Trans. Neural Netw. Learn. Syst.*, vol. 28, no. 3, pp. 584–598, Mar. 2017.

[24] P. J. Werbos, "Consistency of HDP applied to a simple reinforcement learning problem," *Neural Netw.*, vol. 3, no. 2, pp. 179–189, 1990.

[25] J. Si and Y.-T. Wang, "Online learning control by association and reinforcement," *IEEE Trans. Neural Netw.*, vol. 12, no. 2, pp. 264–276, Mar. 2001.

[26] Y. Tang, H. He, J. Wen, and J. Liu, "Power system stability control for a wind farm based on adaptive dynamic programming," *IEEE Trans. Smart Grid*, vol. 6, no. 1, pp. 166–177, Jan. 2015.

[27] C. Mu, D. Wang, and H. He, "Novel iterative neural dynamic programming for data-based approximate optimal control design," *Automatica*, vol. 81, pp. 240–252, Jul. 2017.

[28] J. Liang, G. K. Venayagamoorthy, and R. G. Harley, "Wide-area measurement based dynamic stochastic optimal power flow control for smart grids with high variability and uncertainty," *IEEE Trans. Smart Grid*, vol. 3, no. 1, pp. 59–69, Mar. 2012.

[29] Y. Zhang, X. Ai, J. Fang, J. Wen, and H. He, "Data-adaptive robust optimization method for the economic dispatch of active distribution networks," *IEEE Trans. Smart Grid*, vol. 10, no. 4, pp. 3791–3800, Jul. 2019. doi: 10.1109/TSG.2018.2834952.

[30] Y. Jiang and Z.-P. Jiang, "Robust adaptive dynamic programming with an application to power systems," *IEEE Trans. Neural Netw. Learn. Syst.*, vol. 24, no. 7, pp. 1150–1156, Jul. 2013.

[31] C. Mu, W. Liu, and W. Xu, "Hierarchically adaptive frequency control for an EV-integrated smart grid with renewable energy," *IEEE Trans. Ind. Informat.*, vol. 14, no. 9, pp. 4254–4263, Sep. 2018.

[32] X. Yu and Y. Xue, "Smart grids: A cyber-physical systems perspective," *Proc. IEEE*, vol. 104, no. 5, pp. 1058–1070, May 2016.

[33] K. Takigawa, N. Okada, N. Kuwabara, A. Kitamura, and F. Yamamoto, "Development and performance test of smart power conditioner for value-added PV application," *Solar Energy Mater. Solar Cells*, vol. 75, nos. 3–4, pp. 547–555, 2003.

[34] X. Li, D. Hui, and X. Lai, "Battery energy storage station (BESS)-based smoothing control of photovoltaic (PV) and wind power generation fluctuations," *IEEE Trans. Sustain. Energy*, vol. 4, no. 2, pp. 464–473, Apr. 2013.

[35] T. Zhao and Z. Ding, "Cooperative optimal control of battery energy storage system under wind uncertainties in a microgrid," *IEEE Trans. Power Syst.*, vol. 33, no. 2, pp. 2292–2300, Mar. 2018.

[36] G. O. Suvire, M. G. Molina, and P. E. Mercado, "Improving the integration of wind power generation into AC microgrids using flywheel energy storage," *IEEE Trans. Smart Grid*, vol. 3, no. 4, pp. 1945–1954, Dec. 2012.

[37] M. R. Aghamohammadi and H. Abdolahinia, "A new approach for optimal sizing of battery energy storage system for primary frequency control of islanded microgrid," *Int. J. Elect. Power Energy Syst.*, vol. 54, pp. 325–333, Jan. 2014.

[38] P. C. Sekhar and S. Mishra, "Storage free smart energy management for frequency control in a diesel-PV-fuel cell-based hybrid AC microgrid," *IEEE Trans. Neural Netw. Learn. Syst.*, vol. 27, no. 8, pp. 1657–1671, Aug. 2016.

[39] A. Oudalov, D. Chartouni, and C. Ohler, "Optimizing a battery energy storage system for primary frequency control," *IEEE Trans. Power Syst.*, vol. 22, no. 3, pp. 1259–1266, Aug. 2007.

[40] J.-Y. Kim *et al.*, "Cooperative control strategy of energy storage system and microsources for stabilizing the microgrid during islanded operation," *IEEE Trans. Power Electron.*, vol. 25, no. 12, pp. 3037–3048, Dec. 2010.

[41] B. Ge *et al.*, "Energy storage system-based power control for grid-connected wind power farm," *Int. J. Elect. Power Energy Syst.*, vol. 44, no. 1, pp. 115–122, 2013.

[42] L. Johnston, F. Díaz-González, O. Gomis-Bellmunt, C. Corchero-García, and M. Cruz-Zambrano, "Methodology for the economic optimisation of energy storage systems for frequency support in wind power plants," *Appl. Energy*, vol. 137, pp. 660–669, Jan. 2015.

[43] C. Mu, Y. Zhang, Z. Gao, and C. Sun, "ADP-based robust tracking control for a class of nonlinear systems with unmatched uncertainties," *IEEE Trans. Syst., Man, Cybern., Syst.*, to be published. doi: 10.1109/TSMC.2019.2895692.

[44] W. Guo, F. Liu, J. Si, D. He, R. Harley, and S. Mei, "Online supplementary ADP learning controller design and application to power system frequency control with large-scale wind energy integration," *IEEE Trans. Neural Netw. Learn. Syst.*, vol. 27, no. 8, pp. 1748–1761, Aug. 2016.

[45] D. Xu, J. Liu, X.-G. Yan, and W. Yan, "A novel adaptive neural network constrained control for a multi-area interconnected power system with hybrid energy storage," *IEEE Trans. Ind. Electron.*, vol. 65, no. 8, pp. 6625–6634, Aug. 2018.

[46] T. H. Mohamed, H. Bevrani, A. A. Hassan, and T. Hiyama, "Decentralized model predictive based load frequency control in an interconnected power system," *Energy Convers. Manag.*, vol. 52, no. 2, pp. 1208–1214, 2011.

[47] H. Bevrani, *Robust Power System Frequency Control*. Cham, Switzerland: Springer, 2014.

[48] J. V. Paatero and P. D. Lund, "Effects of large-scale photovoltaic power integration on electricity distribution networks," *Renew. Energy*, vol. 32, no. 2, pp. 216–234, 2007.

[49] A. Kovach and J. Schmid, "Determination of energy output losses due to shading of building-integrated photovoltaic arrays using a raytracing technique," *Solar Energy*, vol. 57, no. 2, pp. 117–124, 1996.

[50] K. Kurokawa, "Realistic values of various parameters for PV system design," *Renew. Energy*, vol. 15, nos. 1–4, pp. 157–164, 1998.

[51] M. C. Alonso-Garcia, J. M. Ruiz, and W. Herrmann, "Computer simulation of shading effects in photovoltaic arrays," *Renew. Energy*, vol. 31, no. 12, pp. 1986–1993, 2006.

[52] Y. Tang, J. Yang, J. Yan, and H. He, "Intelligent load frequency controller using GrADP for island smart grid with electric vehicles and renewable resources," *Neurocomputing*, vol. 170, pp. 406–416, Dec. 2015.

Chaoxu Mu (M'15–SM'18) received the Ph.D. degree in control science and engineering from the School of Automation, Southeast University, Nanjing, China, in 2012. She was a visiting Ph.D. student with the Royal Melbourne Institute of Technology University, Melbourne, VIC, Australia, from 2010 to 2011. She was a Post-Doctoral Fellow with the Department of Electrical, Computer, and Biomedical Engineering, University of Rhode Island, Kingston, RI, USA, from 2014 to 2016. She is currently an Associate Professor with the School of Electrical and Information Engineering, Tianjin University, Tianjin, China. She has authored over 100 journals and conference papers, and coauthored two monographs. Her current research interests include nonlinear system control and optimization, adaptive, and learning systems.

Yong Zhang received the B.S. degree in automation from Tianjin University, Tianjin, China, in 2017, where he is currently pursuing the Ph.D. degree in control engineering with the School of Electrical and Information Engineering. His research interests include adaptive and robust control, adaptive dynamic programming, neural networks, and related applications.

Hongjie Jia (M'04) received the double B.S. degrees in 1996, M.S. degree in 1999, and the Ph.D. degree in 2001 in electric power engineering from Tianjin University, Tianjin, China, respectively, where he became an Associate Professor in 2002, and was promoted as a Professor in 2006. His research interests include power system reliability assessment, stability analysis and control, distribution network planning, and smart grids.

Haibo He (SM'11–F'18) received the B.S. and M.S. degrees in electrical engineering from the Huazhong University of Science and Technology, China, in 1999 and 2002, respectively, and the Ph.D. degree in electrical engineering from Ohio University, USA, in 2006. He is currently the Robert Haas Endowed Chair Professor with the Department of Electrical, Computer, and Biomedical Engineering, University of Rhode Island, USA. He has published one sole-author research book (Wiley), edited one book (Wiley–IEEE), and six conference proceedings (Springer), and has authored and coauthored over 300 peer-reviewed journals and conference papers. His research interests include computational intelligence, machine learning, data mining, and various applications. He was a recipient of the IEEE International Conference on Communications Best Paper Award in 2014, the IEEE CIS Outstanding Early Career Award in 2014, and the National Science Foundation CAREER Award in 2011. He is currently the Editor-in-Chief of the IEEE TRANSACTIONS ON NEURAL NETWORKS AND LEARNING SYSTEMS. He was the General Chair of the IEEE Symposium Series on Computational Intelligence.